

Metal ions modulate the folding and stability of the tumor suppressor protein S100A2

Hugo M. Botelho¹, Michael Koch², Günter Fritz² and Cláudio M. Gomes¹

¹ Instituto de Tecnologia Química e Biológica, Universidade Nova de Lisboa, Portugal

² Fachbereich Biologie, Universität Konstanz, Germany

Keywords

cancer; metals; p53; protein stability; protein structure and folding

Correspondence

C. M. Gomes, Instituto de Tecnologia Química e Biológica, Universidade Nova de Lisboa, Av. da República, EAN, 2780-157 Oeiras, Portugal
Fax: +351 214411277
Tel: +351 214469332
E-mail: gomes@itqb.unl.pt

(Received 26 November 2008, revised 15 January 2009, accepted 19 January 2009)

doi:10.1111/j.1742-4658.2009.06912.x

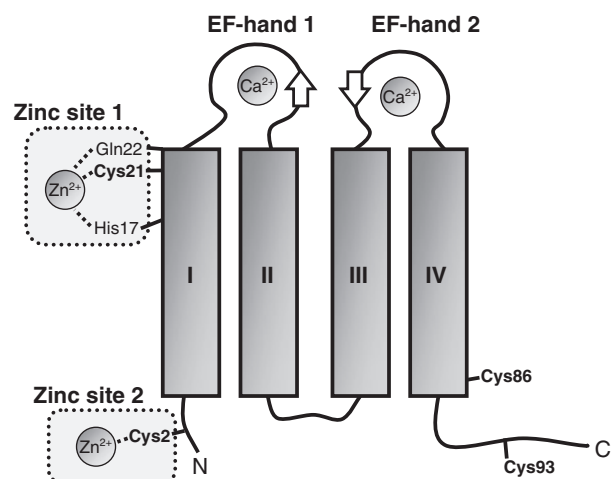
The EF-hand protein S100A2 is a cell cycle regulator involved in tumorigenesis, acting through regulation of the p53 activation state. Metal ion-free S100A2 is homodimeric and contains two Ca²⁺-binding sites and two Zn²⁺-binding sites per subunit, whereby the Zn²⁺ ion binding to one of the sites is coordinated by residues from two homodimers. The effect of selective binding of these metal ions was investigated using site-specific mutants which lacked one or both zinc sites. CD analysis of secondary structure changes on metallation showed that Zn²⁺ binding was associated with a decrease in the secondary structure content, whereas Ca²⁺ had the opposite effect in two of the three S100A2 mutants studied. The energy of unfolding (ΔG_U) of the apo wild-type S100A2 was determined to be 89.9 kJ·mol⁻¹, and the apparent midpoint transition temperature (T_m^{app}) was 58.4 °C. In addition, a detailed study of the urea and thermal unfolding of the S100A2 mutants in different metallation states (apo, Zn²⁺ and Ca²⁺) was performed. Thermal denaturation experiments showed that Zn²⁺ acts as a destabilizer and Ca²⁺ as a stabilizer of the protein conformation. This suggests a synergistic effect between metal binding, protein stability and S100A2 biological activity, according to which Ca²⁺ activates and stabilizes the protein, the opposite being observed on Zn²⁺ binding.

S100A2 is a member of the S100 protein family, the largest subgroup within the superfamily of Ca²⁺-binding EF-hand proteins. Human S100A2 is a 22 kDa homodimer, expressed mainly in the kidney, liver, heart and skeletal muscle [1]. Notably, the cellular localization of S100A2 is restricted to the nucleus [2,3]. S100A2 is a tumour suppressor protein [4], which is down-regulated by promoter hypermethylation in breast and prostate cancer [5,6]. Its tumour suppressor activity is directly linked to p53, which is activated by binding of S100A2, in a Ca²⁺-dependent manner [7] [$K_d(\text{Ca}^{2+}) \sim 100 \mu\text{M}$]. Each S100A2 protomer is composed of two tandem Ca²⁺-binding helix-loop-helix EF-hands [8], the N-terminal one of which has a consensus sequence that is specific to S100 proteins (Scheme 1). As in other cases, the binding of Ca²⁺ to

S100 proteins induces structural changes: helix III rotates by approximately 90°, exposing an interhelical hydrophobic protein interaction site [9–11]. Zn²⁺ ions bind in two surface sites [12]. Site 1 has higher affinity and is composed of Cys21 and probably His17, Gln22 and a solvent molecule. The Zn²⁺ in site 2 is tetra-coordinated by Cys2 from two bridged S100A2 dimers. Both Ca²⁺ and Zn²⁺ are able to bind simultaneously to S100A2, as two Ca²⁺-binding events are detected when titrating the Zn²⁺-saturated protein [12]. Within the S100 family, Zn²⁺ has a unique role in S100A2, whose molecular basis remains to be established: (a) Zn²⁺ binding is not common to all family members and S100A2 exhibits the second highest Zn²⁺ affinity ($K_d = 25 \text{ nM}$; close to S100A3, with $K_d = 4 \text{ nM}$ [13]), making S100A2 a more sensitive sensor for Zn²⁺ than

Abbreviations

C_m , denaturant midpoint transition concentration; T_m^{app} , apparent midpoint transition temperature; ΔG_U , unfolding free energy.



Scheme 1. S100A2 subunit topology, including the location of cysteines and other Zn^{2+} -coordinating residues [8,12]. Boxes represent α -helices and arrows represent β -strands.

for Ca^{2+} ; (b) Zn^{2+} binding to the low-affinity Cys2 site triggers dimer dimerization, which is exclusive to S100A2; (c) physiologically relevant Zn^{2+} concentrations decrease the Ca^{2+} affinity on binding to the same Cys2 site [12]. Indeed, Zn^{2+} -loaded S100A2 is unlikely to activate p53, as physiological free Ca^{2+} concentrations do not exceed 100–300 μM [14–16], and $K_d(Ca^{2+})$ is higher than 800 μM [12]. However, this down-regulation of S100A2 at the post-translational level remains to be determined experimentally.

In order to further explore the interplay between Zn^{2+} and Ca^{2+} binding to S100A2 and to address how metallation affects the protein conformation and

stability, we have investigated the effects of metal ions on the wild-type protein and on mutants lacking one or both Zn^{2+} -binding sites. A detailed knowledge on how Zn^{2+} ions modulate the conformation and stability of S100A2 will contribute to a better understanding of the regulation of protein function by metal ions, in particular as a putative Zn^{2+} sensor.

Results and discussion

Structural changes on Ca^{2+} and Zn^{2+} binding

In order to investigate the effect of Ca^{2+} and Zn^{2+} ions on the structure of S100A2, two previously characterized mutants [12] were studied, together with the wild-type protein. Cysteine residues, which are part of the two S100A2 Zn^{2+} sites (Scheme 1), were replaced by serine residues in mutants C2S and ΔCys (all four cysteines in each subunit were replaced by serine). Therefore, each mutant has a different number of available Zn^{2+} sites: S100A2-wt has two sites, S100A2-C2S only preserves one high-affinity site and S100A2- ΔCys is devoid of specific Zn^{2+} sites. These mutations do not affect Ca^{2+} affinity [12], thus allowing the analysis of the role of Zn^{2+} on binding to the available sites.

These S100A2 mutants were investigated in the apo and holo forms corresponding to different metallated states at 25 °C using far-UV CD (Fig. 1). The CD spectra of all protein preparations are typical of α -helix proteins, with local minima at 208 and 222 nm and local maxima at 195 and 215 nm, in agreement with the ΔCys -S100A2 crystal structure [8] and other

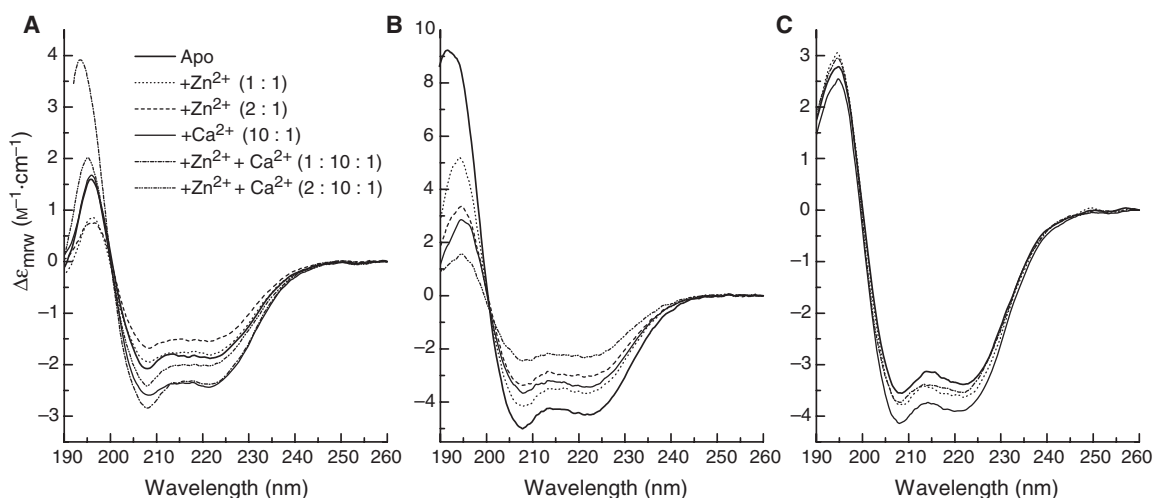


Fig. 1. CD spectra of S100A2 wt (A), C2S (B) and ΔCys (C) in several metal load conditions.

structural data [12,17–20]. This observation also corroborates previous results, indicating that the cysteine replacements do not affect the overall protein fold [12].

Binding of Zn^{2+} to S100A2-wt and S100A2- ΔCys does not elicit significant secondary structure changes (Fig. 1A,C). In the latter case, this is justified by the absence of Zn^{2+} sites, although the far-UV CD spectrum is sensitive to nonspecific Zn^{2+} binding to this mutant (data not shown). However, Zn^{2+} binding to the S100A2-C2S mutant produces a concentration-dependent decrease in secondary structure (Fig. 1B) on addition of one and two Zn^{2+} equivalents, respectively. Binding of Ca^{2+} to S100A2-wt and S100A2- ΔCys results in an increase in the α -helical content (Fig. 1A,C). An opposite effect is observed in the S100A2-C2S mutant (Fig. 1B). The greatest increase in secondary structure occurs when both Ca^{2+} and Zn^{2+} are added to the wild-type protein (Fig. 1A).

In order to investigate the possibility that the observed variations in secondary structure resulting from metallation with Ca^{2+} and Zn^{2+} are caused by a change in the oligomeric state of the proteins or aggregation, we carried out dynamic light scattering studies. We detected average molecular diameters of around 5–5.5 nm, irrespective of mutation or metal load up to stoichiometric metal binding, consistent with the structure of apo S100A2 [8]. However, tetramerization occurs at higher zinc to protein ratios [12]. The slightly larger diameter of S100A2-wt + 2 Eq. Zn^{2+} (6.4 nm) could be suggestive of partial tetramerization (Fig. S1).

Chemical stability of holo and apo S100A2 proteins

The conformational stability of S100A2-wt and mutants, in the apo and distinct metallated states, was investigated by performing urea denaturation experiments. For all proteins, the far-UV CD spectra obtained at increasing urea concentrations denoted a transition from α -helix to random conformations, apparently via intermediate β -sheet structures (Fig. 2A).

To extract thermodynamic information from protein denaturation curves, the unfolding mechanism needs to be known. For single-domain dimeric proteins, such as S100A2, this process may be hypothesized to comprise two steps: the dissociation of the native dimer into folded monomers, which, in turn, undergo denaturation. However, the chemical denaturation of S100A2 could be rationalized using a simple two-state unfolding mechanism, where the unfolding of the folded dimer (F_2) yields denatured monomer (U) directly:



This mechanism is supported by several criteria: (a) no intermediate species were detected in any of the denaturation curves (Fig. 2); (b) the denaturant mid-point transition concentration (C_m) of apo S100A2-wt and S100A2- ΔCys increased with protein concentration (not shown); and (c) the denaturation curves of the latter mutant, obtained by CD and intrinsic tyrosine fluorescence, were superimposable (not shown) [21]. Accordingly, the mechanism in Eqn (1) was employed to derive the thermodynamic parameters, using the formalism established by Grant *et al.* [22] (Fig. 2B–D; Tables 1 and 2).

A two-state unfolding mechanism has also been reported for human S100B [23] and porcine S100A12 [24]. All stability parameters extracted from denaturation curves (Fig. 3B–D; Tables 1 and 2) were found to be within the typical range for small dimeric proteins [25] and, in particular, in accordance with thermodynamic data reported on human S100B [23] and porcine S100A12 [24].

The unfolding free energy (ΔG_U) value of apo S100A2-wt was $89.9 \text{ kJ}\cdot\text{mol}^{-1}$ and S100A2-C2S and S100A2- ΔCys were destabilized by -2.3 and $-5.8 \text{ kJ}\cdot\text{mol}^{-1}$ with respect to the wild-type (Table 1). The data suggest identical unfolding mechanisms for all three apo proteins, as neither the transition cooperativity (m index) nor the shape of the far-UV CD spectra at different urea concentrations (not shown) was significantly affected. Thus, meaningful information on the thermodynamic stability of the Ca^{2+} - and Zn^{2+} -loaded mutants can be retrieved from the analysis of metallation effects within the background of the same mutation (Table 2). With the exception of Zn^{2+} -loaded S100A2- ΔCys , which is devoid of Zn^{2+} sites, the metallated states exhibit a decreased cooperativity of the unfolding transition. This suggests that, in such cases, the amount of surface area being exposed during urea unfolding is lower than in the apo state, and/or that metal binding increases the subpopulations of native protein with slightly different conformations.

However, occupation of the metal sites by Zn^{2+} or Ca^{2+} ions has a distinct effect on protein stability. Metallation of the high-affinity Zn^{2+} site of S100A2-C2S has a destabilizing effect of $-3.9 \text{ kJ}\cdot\text{mol}^{-1}$, whereas the same stoichiometric Zn^{2+} amount destabilizes the wild-type protein by $-14.2 \text{ kJ}\cdot\text{mol}^{-1}$. This large destabilization probably arises from residual binding of Zn^{2+} to the low-affinity site, which is known to promote the exposure of hydrophobic

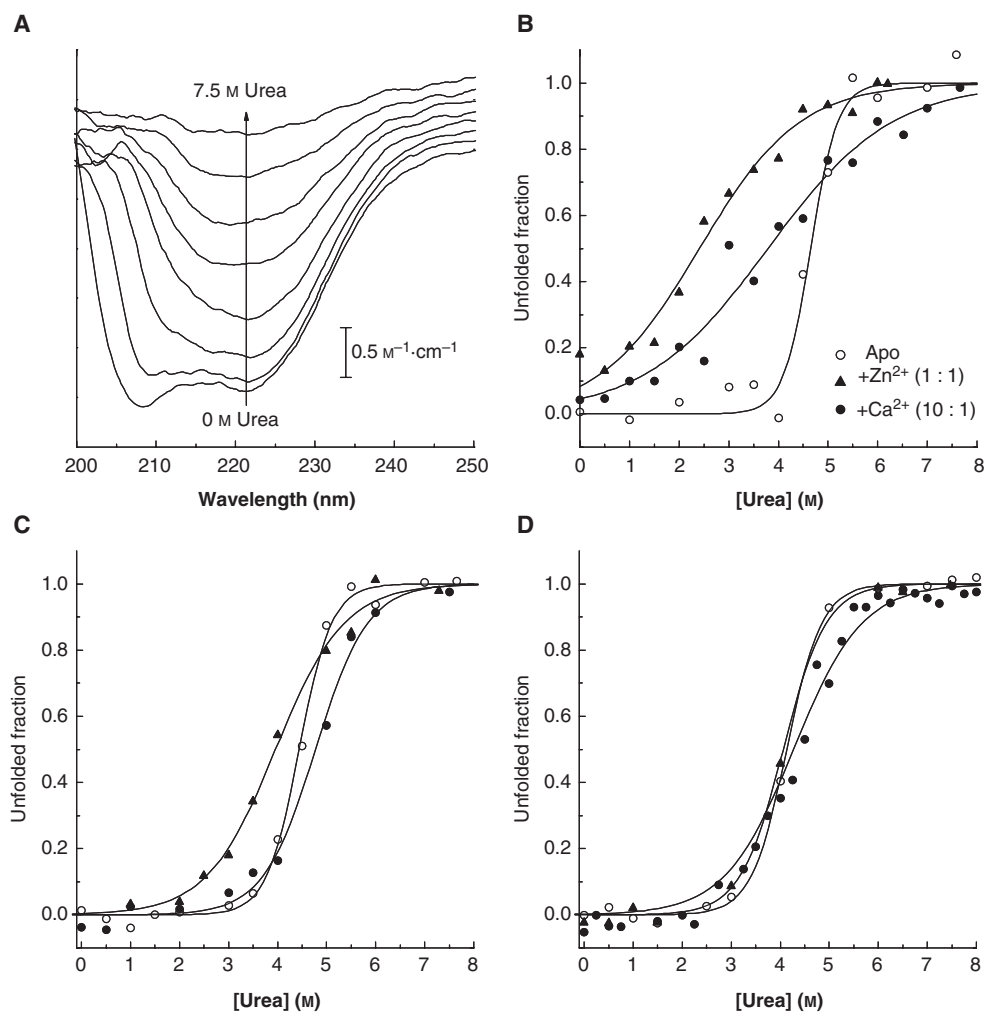


Fig. 2. CD-monitored urea chemical denaturation curves of S100A2. Representative spectra of Ca²⁺-loaded S100A2-wt at increasing urea concentration (0–7.5 M), as indicated by the arrow (A). Displacement: 0.1 M⁻¹·cm⁻¹. Denaturation curves of wt (B), C2S (C) and S100A2-ΔCys (D) in several metal load conditions.

Table 1. Thermodynamic stability parameters for the apo S100A2 variants.

	Apo			$\Delta\Delta G_U^a$ (kJ·mol ⁻¹)
	[Urea] _{1/2} (M)	ΔG_U (kJ·mol ⁻¹)	m (kJ·mol ⁻¹ ·M ⁻¹)	
wt	4.7	89.9	13.0	–
C2S	4.5	78.9	11.2	–2.3
ΔCys	4.2	71.8	10.3	–5.8

^a $\Delta\Delta G_U = \Delta[Urea]_{1/2} \times m_{\text{average}}$ [36].

surfaces [12]. In contrast, binding of Ca²⁺ stabilizes the mutants by +0.8 or +2.4 kJ·mol⁻¹, but destabilizes the wild-type protein by –5.2 kJ·mol⁻¹. Some point mutations are known to exert long-range effects in

S100 proteins because of their effect in hydrogen bond networks [26]. It is reasonable to hypothesize that the same applies to the S100A2 mutants under study. The lower unfolding cooperativity of the Ca²⁺-loaded samples suggests a concurrent opening of the EF-hands, resulting in a decreased exposure of the surface area during unfolding.

Thermal stability of holo and apo S100A2 proteins

We have complemented the chemical denaturation study by performing analogous temperature-induced unfolding assays. For all proteins, increasing the temperature results in a progressive α -helix to random coil transition (Fig. 3A). No notorious protein precipita-

Table 2. Thermodynamic stability parameters for the S100A2 variants in the apo, Zn²⁺ (1 : 1) and Ca²⁺ (10 : 1) metallated states.

	S100A2-wt				S100A2-C2S				S100A2-ΔCys			
	[Urea] _{1/2} (M)	ΔG _U (kJ·mol ⁻¹)	<i>m</i> (kJ· mol ⁻¹ ·M ⁻¹)	ΔΔG _U ^a (kJ·mol ⁻¹)	[Urea] _{1/2} (M)	ΔG _U (kJ· mol ⁻¹)	<i>m</i> (kJ· mol ⁻¹ ·M ⁻¹)	ΔΔG _U ^a (kJ·mol ⁻¹)	[Urea] _{1/2} (M)	ΔG _U (kJ· mol ⁻¹)	<i>m</i> (kJ· mol ⁻¹ ·M ⁻¹)	ΔΔG _U ^a (kJ·mol ⁻¹)
Apo	4.7	89.9	13.0	–	4.5	78.9	11.2	–	4.2	71.8	10.3	–
+Zn ²⁺	2.5	35.1	3.5	–14.2	4.0	50.1	5.3	–3.9	4.1	68.2	9.7	–0.8
+Ca ²⁺	3.9	40.3	2.9	–5.2	4.8	62.4	7.0	+2.4	4.3	51.8	5.3	+0.8

^aΔΔG_U = Δ[Urea]_{1/2} × *m*_{average} [36].

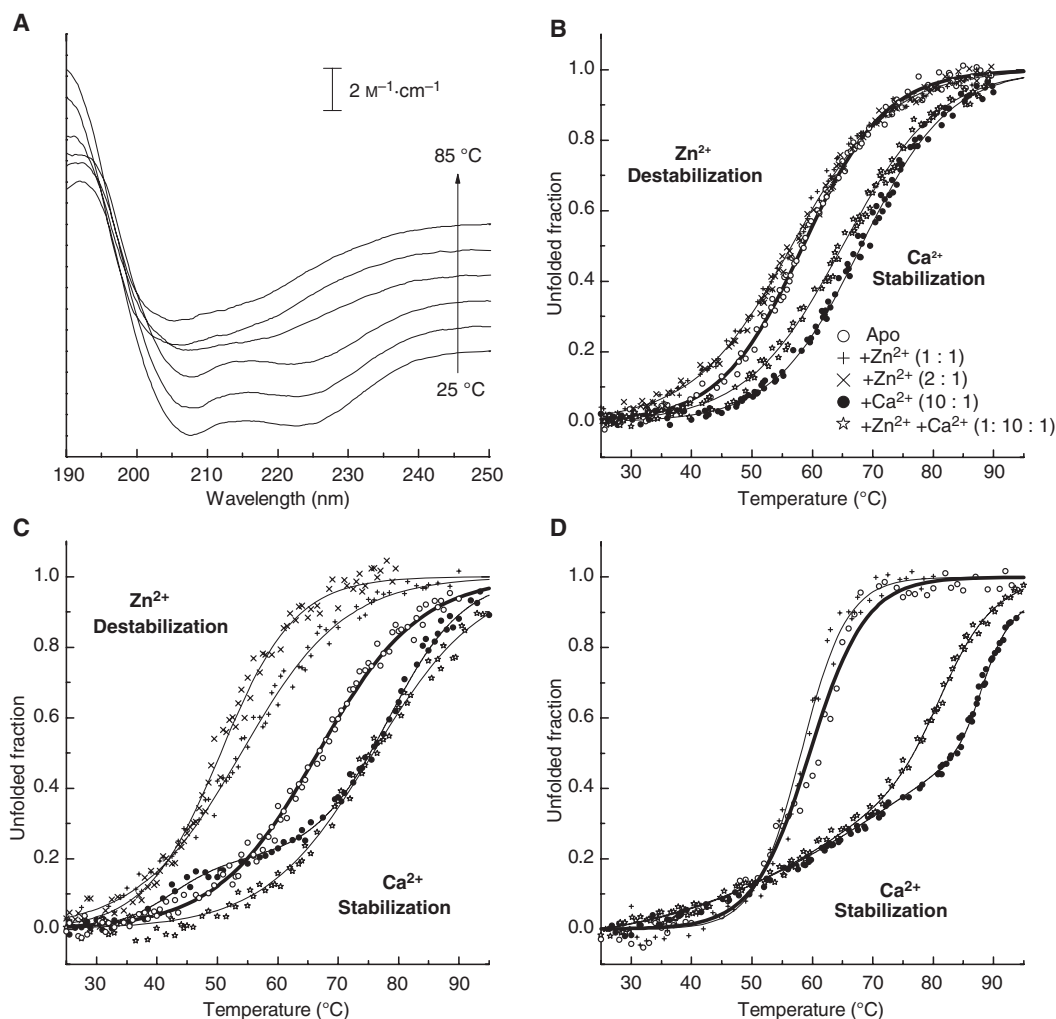


Fig. 3. CD-monitored thermal denaturation of S100A2. Representative spectra of apo S100A2-wt at increasing temperatures (25–85 °C), as indicated by the arrow (A). Displacement: 1.2 M⁻¹·cm⁻¹. The spectra of the native and denatured form are representative for all thermal denaturations. Thermal denaturation curves of wt (B), C2S (C) and S100A2-ΔCys (D) in several metal load conditions.

tion was observed, suggesting that other non-reversible modifications may occur at high temperatures. This differed from urea unfolding, precluding a detailed thermodynamic analysis, and is suggestive of distinct pathways for chemical and thermal unfolding. Never-

theless, a comparison of the apparent midpoint transition temperature (T_m^{app}), obtained for the different metallated states, is very informative with respect to the effect of each metal on the stability of each protein mutant (Table 3).

Table 3. Apparent T_m values determined from CD-monitored thermal denaturation curves of S100A2 variants. The aggregation of S100A2- Δ Cys incubated with 2 Eq. Zn^{2+} occurs during the temperature ramp. n.d., not determined.

	T_m^{app} (°C)					
	Apo	+ Zn^{2+} (1 : 1)	+ Zn^{2+} (2 : 1)	+ Ca^{2+} (10 : 1)	+ Zn^{2+} + Ca^{2+} (1 : 10 : 1)	+ Zn^{2+} + Ca^{2+} (2 : 10 : 1)
wt	58.4	56.6	56.6	68.1	65.0	n.d.
C2S	66.6	53.9	50.6	~ 42 > 80	n.d.	76.8
Δ Cys	59.5	58.1	Aggregates	~ 75 > 85	~ 65 > 81	Aggregates

Apo S100A2-wt and S100A2- Δ Cys have very similar T_m^{app} values of 58.4 and 59.5 °C, respectively, which are lower than the T_m^{app} value of 66.6 °C of S100A2-C2S. The outlying behaviour of apo S100A2-C2S may result from long-range mutation effects [26], which are not observed in the other mutants. Considering these aspects, the relevant comparisons will relate to differences observed on selective metallation, within the same mutant.

Interestingly, Ca^{2+} and Zn^{2+} metallation showed antagonistic effects in thermal stability (Fig. 3B–D). Zn^{2+} ions had a destabilizing effect, which was concentration dependent in S100A2-C2S, in agreement with the observed decrease in secondary structure content. The destabilization arose from the metal-induced conformational change, because no kinetic distortions affected the Zn^{2+} -induced conformational destabilization. Binding of Zn^{2+} to the unfolded state could have caused a shift in the equilibrium, but this effect is only significant at a large excess of Zn^{2+} [27], which was not the case in our experiments (a maximum of one or two Zn^{2+} equivalents was used). In addition, the kinetics of thermal denaturation did not vary significantly between apo and Zn^{2+} -loaded S100A2-C2S (see Experimental procedures). The Ca^{2+} -loaded proteins exhibited an increased T_m^{app} value, although the mutants had at least one unfolding intermediate in the denaturation curves. The increased stability of Ca^{2+} -loaded proteins probably resides in the electrostatic compensation at the negatively charged Ca^{2+} -binding sites.

The opposite effect of the two metals on thermal stability prompted us to study Ca^{2+} and Zn^{2+} ions in combination. In S100A2-wt, where all binding sites are available, metal ion effects are dominated by the Ca^{2+} contribution. Indeed, an intermediate stability with respect to Zn^{2+} destabilization ($\Delta T_m^{app} = -1.8$ °C) and Ca^{2+} stabilization ($\Delta T_m^{app} = +9.7$ °C) was determined when Zn^{2+} and Ca^{2+} were combined ($\Delta T_m^{app} = +6.6$ °C) (Fig. 4B).

It can be hypothesized that the two thermal transitions of Ca^{2+} -loaded S100A2-C2S correspond to the

unfolding of different structural regions, the transition at approximately 42 °C (Fig. 3C) corresponding to unfolding at the N-terminal EF-hand, as it is stabilized by Zn^{2+} binding at the adjacent site I (Scheme 1). Such stabilization is not observed in S100A2- Δ Cys (Fig. 3D), which has no specific Zn^{2+} sites. In this case, nonspecific Zn^{2+} binding is likely to result in destabilization without changing the shape of the denaturation curve.

Complementary to the CD experiments, the thermal denaturation of S100A2- Δ Cys was followed by FT-IR. The absorbance change at the amide I (1600–1700 cm^{-1}) and amide II (1500–1600 cm^{-1}) bands was used to probe the unfolding, monitoring secondary structure elements. As shown above, this mutant does not bind Zn^{2+} , so we carried out a study of the apo and Ca^{2+} -loaded forms of Δ Cys-S100A. In both conditions, denaturation consisted of transition from α -helical (~ 1650 and 1550 cm^{-1}) to random (1525 cm^{-1}) and β -structures (~ 1622 cm^{-1}) (Fig. 4A,C). The latter vibration is associated with intermolecular β -sheets and aggregation. The formation of insoluble β -sheet-containing aggregates is most certainly an important contributor to the irreversibility of the thermal denaturation. The denaturation curves of the above-mentioned structural elements are compatible with the CD results, and further corroborate a two-state unfolding process. All secondary structure elements of apo S100A2- Δ Cys exhibit similar profiles, with T_m^{app} ranging from 67 to 71 °C. The unfolding of the secondary structure elements of Ca^{2+} -loaded S100A2- Δ Cys also occurs simultaneously, and at $T_m^{app} > 80$ °C. Again, a very good agreement with the far-UV CD data is observed.

Conclusions

In this work, we have characterized how the conformation and stability of S100A2 are influenced by the specific metal ions Zn^{2+} and Ca^{2+} . In particular, considering the unique role of Zn^{2+} in S100A2, we have dissected the contribution arising from Zn^{2+} binding

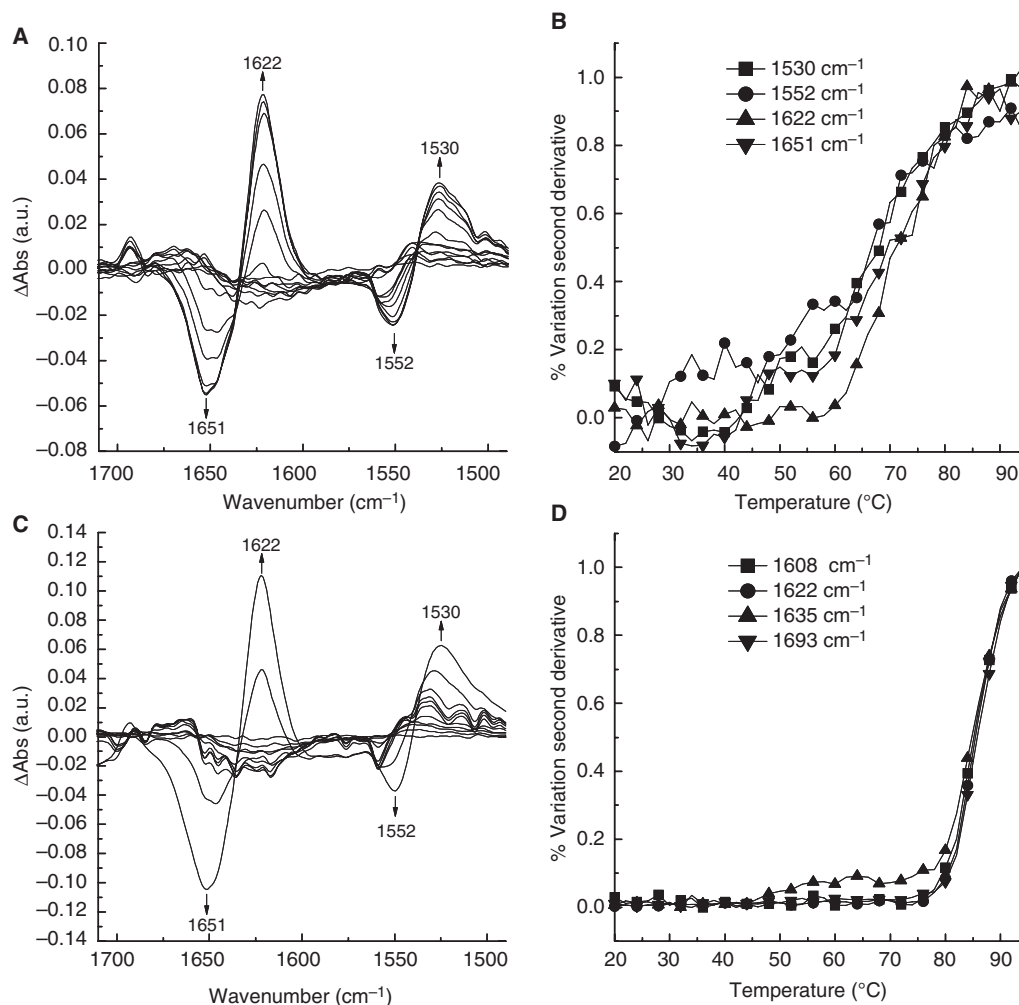


Fig. 4. Attenuated total reflectance FT-IR-monitored thermal denaturation of S100A2- Δ Cys in the apo (A, B) and Ca²⁺-loaded (C, D) forms. Representative difference spectra at increasing temperature (20–94 °C), as indicated by the arrows (A and C). Thermal denaturation curves for the apo (B) and Ca²⁺-loaded (D) proteins are derived from the second-derivative trend with temperature.

using two mutants, with selective disruption of the low- and high-affinity Zn²⁺-binding sites, as models. We have observed that the S100A2 conformation is sensitive to the metallation state, and that the rearrangements resulting from metal binding preserve the overall fold of the protein. Chemical denaturation suggests that both Zn²⁺- and Ca²⁺-associated conformational changes facilitate the accessibility of urea to the protein core, leading to destabilization. Thermal denaturation suggests that Zn²⁺ and Ca²⁺ regulate protein thermal stability antagonistically, Zn²⁺ being a destabilizer and Ca²⁺ a stabilizer. Similarly, Ca²⁺ stabilizes and Cu²⁺ destabilizes S100A13 towards thermal perturbation [28]. Other studies highlight distinct regulatory mechanisms of S100 proteins by metal ions. For example, Ca²⁺ was shown to stabilize human S100B towards denaturation by guanidinium hydrochloride

[22], and porcine S100A12 was shown to be stabilized by Ca²⁺ and Zn²⁺ towards thermal denaturation [24]. The behaviour of Zn²⁺-Ca²⁺-loaded S100A2 in the thermal unfolding experiments indicates that Ca²⁺ can at least partially revert the conformational destabilization triggered by Zn²⁺ binding to the high-affinity site.

These effects of metal ions on S100A2 folding and stability contribute to a better understanding of the Ca²⁺- and Zn²⁺-dependent regulation of the protein. In the Ca²⁺-loaded state, S100A2 binds and activates p53 [7]. However, Zn²⁺ negatively regulates the affinity of S100A2 for Ca²⁺ binding [12], which might disable the Ca²⁺ signal, resulting in a blockage of p53 activation. The mechanism of how Zn²⁺ may decrease the Ca²⁺ affinity remained unresolved in our previous study [12]. The results of the present

work reveal that the decrease in Ca^{2+} affinity through Zn^{2+} is presumably a result of the general destabilization of the protein. Further contributions might come from the exposure of a hydrophobic surface on Zn^{2+} binding [12], making additional exposure of the hydrophobic surface induced by Ca^{2+} less favourable.

Zn^{2+} binding to close homologues of S100A2, such as S100A3 [13] and S100A4 (G. Fritz and M. Koch, unpublished data), also occurs mainly via cysteine residues. It remains to be shown whether Zn^{2+} binding to S100A3 and S100A4 also results in a decrease in protein stability. In S100A3, Zn^{2+} binding causes the loss of approximately 40% of the α -helical structure [13], supporting destabilization of the protein. In contrast with S100A2, other S100 proteins, such as S100A12 and S100B, display an increased Ca^{2+} affinity on Zn^{2+} binding [29,30]. Future investigations might show whether, in these S100 proteins, Zn^{2+} increases the conformational stability, thereby facilitating the Ca^{2+} conformational change.

Together, the data presented here provide new insights into the mechanism of Zn^{2+} - and Ca^{2+} -dependent activation of S100 proteins. The antagonistic effect of Zn^{2+} and Ca^{2+} in the control of S100A2 stability provides a molecular rationale for the action of both metal ions. Our results allow the formulation of the following hypothesis: in tissues expressing S100A2, the Zn^{2+} imbalance which arises in some cancers may contribute to enhanced cell proliferation through destabilization of S100A2. This mechanism would impair the interaction with p53, and disrupt subsequent downstream cell cycle regulation. Indeed, Zn^{2+} transporters are upregulated in breast carcinoma and pancreatic tumours [31,32] leading to elevated Zn^{2+} levels [33–35], which may impair Ca^{2+} binding to S100A2 [12]. Current work in our laboratories will allow the testing of this hypothesis.

Experimental procedures

Proteins

Wild-type human S100A2 and mutants C2S and ΔCys (C2S-C21S-C86S-C93S) were expressed in *Escherichia coli* and purified to homogeneity, as described elsewhere [12]; 2 mM Tris/HCl, pH 7.0, was used throughout. All solutions were prepared in Chelex (Sigma, Steinheim, Germany)-treated water and buffers were oxygen free. It is noteworthy that previous studies have determined that the cysteine to serine substitutions do not compromise the overall fold [12,18].

Preparation of apo and metal ion-loaded mutants

The proteins containing cysteines were reduced prior to all experiments, as described elsewhere [12], and quantified spectrophotometrically ($\epsilon^{275,\text{wt}} = 3050 \text{ M}^{-1}\cdot\text{cm}^{-1}$, $\epsilon^{280,\text{C2S}} = 3105 \text{ M}^{-1}\cdot\text{cm}^{-1}$ and $\epsilon^{280,\Delta\text{Cys}} = 2980 \text{ M}^{-1}\cdot\text{cm}^{-1}$). Zn^{2+} was added as one or two molar equivalents to the S100A2 monomer in order to fill only the high-affinity or both sites. Ca^{2+} was added as 10 molar equivalents. Metal chloride salts were used (Fluka, Steinheim, Germany). For CD and fluorescence measurements in the presence of metals, the protein samples were equilibrated for 1 h at 4 °C after the addition of the metal.

CD spectroscopy

CD measurements were recorded in a Jasco J-815 spectropolarimeter equipped with a Peltier-controlled thermostatic cell support. Thermal denaturation experiments were carried out by increasing the temperature from 25 to 95 °C at a heating rate of 1 °C \cdot min $^{-1}$. Changes in the CD signal at 222 nm were plotted as a function of temperature, and T_m^{app} was determined from fitting to single or the sum of two sigmoidal curves. The protein concentration was 0.1 mg \cdot mL $^{-1}$. Thermal denaturation was irreversible. However, no kinetically controlled steps affected protein unfolding, as T_m^{app} was independent of the heating rate for S100A2- ΔCys (not shown), as observed in a system undergoing reversible unfolding. Therefore, the determined T_m^{app} values are those of a pseudo-equilibrium and are suitable for comparative purposes between the mutants studied.

The thermal denaturation kinetics (25–65 °C temperature jumps) of the single Zn^{2+} site mutant S100A2-C2S were investigated in the apo and Zn^{2+} -loaded (1 : 1) state, following the decay of the CD signal at 225 nm. This mutant preserves Zn^{2+} site 1, present in all S100A2 mutants, and does not tetramerize because it lacks site 2. The protein concentration was 0.2 mg \cdot mL $^{-1}$.

Fluorescence spectroscopy

Intrinsic tyrosine fluorescence measurements were performed on a Varian (Palo Alto, CA, USA) Cary Eclipse instrument. The temperature was kept at 25 °C by a Peltier-controlled thermostatic cell support. Emission spectra on 275 nm excitation were recorded using 10 nm excitation and emission slits.

Attenuated total reflectance FT-IR spectroscopy

Attenuated total reflectance FT-IR measurements were performed in a Bruker (Ettlingen, Germany) IFS 66/S spectrometer equipped with a nitrogen-cooled MCT detector using a thermostatically controlled Harrick (Ossining, NY,

USA) BioATRCcell II. Spectra were acquired at 4 cm^{-1} resolution. Difference spectra were calculated after vector normalization of the absorbance in the amide I–amide II region. Different metallated forms of S100A2 mutants were prepared by *in situ* dialysis using the manufacturer's accessory. Apo protein samples ($\sim 10\text{ mg}\cdot\text{mL}^{-1}$) were dialysed at $20\text{ }^\circ\text{C}$ against 5 mM Tris/HCl, pH 7, 23 mM NaCl. Ten molar equivalents of Ca^{2+} were added to the same buffer with the NaCl concentration adjusted to equalize the ionic strength.

Thermal denaturation experiments involved increasing the cell temperature from 20 to $94\text{ }^\circ\text{C}$. The heating rate was discontinuous (average $\sim 1.3\text{ }^\circ\text{C}\cdot\text{min}^{-1}$) as a result of step-wise spectrum acquisition (every $2\text{ }^\circ\text{C}$; acquisition time, 1 min). Denaturation curves were obtained by plotting spectra second-derivative values at local maxima or minima as a function of temperature.

Chemical denaturation

Protein unfolding was studied by monitoring the variation in CD at 222 nm , or fluorescence intensity at 305 nm , at $25\text{ }^\circ\text{C}$, as a function of urea concentration. Fresh urea (Riedel-de Haën, Seelze, Germany) solutions were used for every assay and the rigorous concentration was determined using refractive index measurements [36]. Apo or metallated protein samples ($0.1\text{ mg}\cdot\text{mL}^{-1}$) were incubated for 2 h at room temperature for complete chemical denaturation. The influence of protein concentration on C_m was assessed in the $0.08\text{--}0.25\text{ mg}\cdot\text{mL}^{-1}$ range. Denaturation was reversible for all cases, as urea dilution of the completely denatured protein yielded protein with native state spectra.

Dynamic light scattering

The molecular diameters of S100A2 mutants in different metallation conditions ($0.1\text{ mg}\cdot\text{mL}^{-1}$) were assessed using a Malvern Instruments (Malvern, UK) Zetasizer Nano ZS instrument equipped with a 633 nm laser. The temperature was kept at $25\text{ }^\circ\text{C}$ using a Peltier-controlled thermostatic cell support. Before each measurement, samples were filtered through a $0.22\text{ }\mu\text{m}$ membrane. For each time measurement, the backscattered light (173°) from fourteen 10 s accumulations was averaged. The results were analysed with Malvern Instruments DTS software using a multimodal fit with quadratic weighting and 0.01 regularizer. Size results are from the Mie theory-derived volume distribution of sizes. When available, error bars are the standard deviations from at least three replicate measurements.

Acknowledgements

This work was supported by grants POCTI/QUI/45758 and PTDC/QUI/70101 (to CMG) from the

Fundação para a Ciência e a Tecnologia (FCT/MCTES, Portugal), and DAAD D/07/13610 PPP (to GF and MK). CMG and GF are recipients of a CRUP/DAAD collaborative grant A-15/08. HMB is a recipient of a PhD fellowship (SFRH/BD/31126/2006) from Fundação para a Ciência e a Tecnologia (FCT/MCTES, Portugal).

References

- 1 Glenney JR Jr, Kindy MS & Zokas L (1989) Isolation of a new member of the S100 protein family: amino acid sequence, tissue, and subcellular distribution. *J Cell Biol* **108**, 569–578.
- 2 Mueller A, Bachi T, Höchli M, Schäfer BW & Heizmann CW (1999) Subcellular distribution of S100 proteins in tumor cells and their relocation in response to calcium activation. *Histochem Cell Biol* **111**, 453–459.
- 3 Mandinova A, Atar D, Schäfer BW, Spiess M, Aebi U & Heizmann CW (1998) Distinct subcellular localization of calcium binding S100 proteins in human smooth muscle cells and their relocation in response to rises in intracellular calcium. *J Cell Sci* **111**, 2043–2054.
- 4 Lee SW, Tomasetto C & Sager R (1991) Positive selection of candidate tumor-suppressor genes by subtractive hybridization. *Proc Natl Acad Sci USA* **88**, 2825–2829.
- 5 Pedrocchi M, Schäfer BW, Mueller H, Eppenberger U & Heizmann CW (1994) Expression of Ca(2+)-binding proteins of the S100 family in malignant human breast-cancer cell lines and biopsy samples. *Int J Cancer* **57**, 684–690.
- 6 Rehman I, Cross SS, Catto JW, Leiblich A, Mukherjee A, Azzouzi AR, Leung HY & Hamdy FC (2005) Promoter hyper-methylation of calcium binding proteins S100A6 and S100A2 in human prostate cancer. *Prostate* **65**, 322–330.
- 7 Mueller A, Schäfer BW, Ferrari S, Weibel M, Makek M, Höchli M & Heizmann CW (2005) The calcium-binding protein S100A2 interacts with p53 and modulates its transcriptional activity. *J Biol Chem* **280**, 29186–29193.
- 8 Koch M, Diez J & Fritz G (2008) Crystal structure of Ca^{2+} -free S100A2 at $1.6\text{-}\text{Å}$ resolution. *J Mol Biol* **378**, 931–940.
- 9 Fritz G & Heizmann CW (2004) 3D structures of the calcium and zinc binding S100 proteins. In *Handbook of Metalloproteins* (Messerschmidt A, Huber R, Poulos T & Wiegardt K, eds), pp. 529–540. John Wiley & Sons, Chichester.
- 10 Heizmann CW & Cox JA (1998) New perspectives on S100 proteins: a multi-functional Ca(2+)-, Zn(2+)- and Cu(2+)-binding protein family. *Biometals* **11**, 383–397.

- 11 Lewit-Bentley A & Rety S (2000) EF-hand calcium-binding proteins. *Curr Opin Struct Biol* **10**, 637–643.
- 12 Koch M, Bhattacharya S, Kehl T, Gimona M, Vasak M, Chazin W, Heizmann CW, Kroneck PM & Fritz G (2007) Implications on zinc binding to S100A2. *Biochim Biophys Acta* **1773**, 457–470.
- 13 Fritz G, Mittl PR, Vasak M, Grutter MG & Heizmann CW (2002) The crystal structure of metal-free human EF-hand protein S100A3 at 1.7-Å resolution. *J Biol Chem* **277**, 33092–33098.
- 14 Alonso MT, Villalobos C, Chamero P, Alvarez J & Garcia-Sancho J (2006) Calcium microdomains in mitochondria and nucleus. *Cell Calcium* **40**, 513–525.
- 15 Jones HE, Holland IB, Baker HL & Campbell AK (1999) Slow changes in cytosolic free Ca^{2+} in *Escherichia coli* highlight two putative influx mechanisms in response to changes in extracellular calcium. *Cell Calcium* **25**, 265–274.
- 16 Knight MR, Campbell AK, Smith SM & Trewavas AJ (1991) Recombinant aequorin as a probe for cytosolic free Ca^{2+} in *Escherichia coli*. *FEBS Lett* **282**, 405–408.
- 17 Franz C, Durussel I, Cox JA, Schafer BW & Heizmann CW (1998) Binding of Ca^{2+} and Zn^{2+} to human nuclear S100A2 and mutant proteins. *J Biol Chem* **273**, 18826–18834.
- 18 Koch M, Diez J & Fritz G (2006) Purification and crystallization of the human EF-hand tumour suppressor protein S100A2. *Acta Crystallogr Sect F Struct Biol Cryst Commun* **62**, 1120–1123.
- 19 Randazzo A, Acklin C, Schäfer BW, Heizmann CW & Chazin WJ (2001) Structural insight into human $\text{Zn}(2+)$ -bound S100A2 from NMR and homology modeling. *Biochem Biophys Res Commun* **288**, 462–467.
- 20 Stradal TB, Troxler H, Heizmann CW & Gimona M (2000) Mapping the zinc ligands of S100A2 by site-directed mutagenesis. *J Biol Chem* **275**, 13219–13227.
- 21 Bosshard HR (2005) Concurrent association and folding of small oligomeric proteins. In *Protein Folding Handbook* (Buchner J & Kiefhaber T, eds), pp. 965–997. Wiley-VCH Verlag GmbH, Weinheim.
- 22 Grant SK, Deckman IC, Culp JS, Minnich MD, Brooks IS, Hensley P, Debouck C & Meek TD (1992) Use of protein unfolding studies to determine the conformational and dimeric stabilities of HIV-1 and SIV proteases. *Biochemistry* **31**, 9491–9501.
- 23 Ferguson PL & Shaw GS (2002) Role of the N-terminal helix I for dimerization and stability of the calcium-binding protein S100B. *Biochemistry* **41**, 3637–3646.
- 24 Garcia AF, Garcia W, Nonato MC & Araujo AP (2008) Structural stability and reversible unfolding of recombinant porcine S100A12. *Biophys Chem* **134**, 246–253.
- 25 Mei G, Di Venere A, Rosato N & Finazzi-Agro A (2005) The importance of being dimeric. *FEBS J* **272**, 16–27.
- 26 Nelson MR, Thulin E, Fagan PA, Forsen S & Chazin WJ (2002) The EF-hand domain: a globally cooperative structural unit. *Protein Sci* **11**, 198–205.
- 27 Conejero-Lara F, Mateo PL, Aviles FX & Sanchez-Ruiz JM (1991) Effect of Zn^{2+} on the thermal denaturation of carboxypeptidase B. *Biochemistry* **30**, 2067–2072.
- 28 Sivaraja V, Kumar TK, Rajalingam D, Graziani I, Prudovsky I & Yu C (2006) Copper binding affinity of S100A13, a key component of the FGF-1 nonclassical copper-dependent release complex. *Biophys J* **91**, 1832–1843.
- 29 Baudier J, Glasser N & Gerard D (1986) Ions binding to S100 proteins. I. Calcium- and zinc-binding properties of bovine brain S100 alpha alpha, S100a (alpha beta), and S100b (beta beta) protein: Zn^{2+} regulates Ca^{2+} binding on S100b protein. *J Biol Chem* **261**, 8192–8203.
- 30 Dell'Angelica EC, Schleicher CH & Santome JA (1994) Primary structure and binding properties of calgranulin C, a novel S100-like calcium-binding protein from pig granulocytes. *J Biol Chem* **269**, 28929–28936.
- 31 Li M, Zhang Y, Liu Z, Bharadwaj U, Wang H, Wang X, Zhang S, Liuzzi JP, Chang SM, Cousins RJ *et al.* (2007) Aberrant expression of zinc transporter ZIP4 (SLC39A4) significantly contributes to human pancreatic cancer pathogenesis and progression. *Proc Natl Acad Sci USA* **104**, 18636–18641.
- 32 Taylor KM, Morgan HE, Smart K, Zahari NM, Pumford S, Ellis IO, Robertson JF & Nicholson RI (2007) The emerging role of the LIV-1 subfamily of zinc transporters in breast cancer. *Mol Med* **13**, 396–406.
- 33 Cui Y, Vogt S, Olson N, Glass AG & Rohan TE (2007) Levels of zinc, selenium, calcium, and iron in benign breast tissue and risk of subsequent breast cancer. *Cancer Epidemiol Biomarkers Prev* **16**, 1682–1685.
- 34 Geraki K, Farquharson MJ & Bradley DA (2002) Concentrations of Fe, Cu and Zn in breast tissue: a synchrotron XRF study. *Phys Med Biol* **47**, 2327–2339.
- 35 Ionescu JG, Novotny J, Stejskal V, Latsch A, Blau-rock-Busch E & Eisenmann-Klein M (2006) Increased levels of transition metals in breast cancer tissue. *Neuroendocrinol Lett* **27**(Suppl. 1), 36–39.
- 36 Pace CN, Shirley BA & Thomson JA (1990) Measuring the conformational stability of a protein. In *Protein Structure – A Practical Approach* (Creighton TE, ed.), pp. 311–330. IRL Press, Oxford.

Supporting information

The following supplementary material is available:

Fig. S1. Molecular diameter of the apo and metallated S100A2 variants as assessed by dynamic light scattering.

This supplementary material can be found in the online version of this article.

Please note: Wiley-Blackwell is not responsible for the content or functionality of any supplementary materials supplied by the authors. Any queries (other than missing material) should be directed to the corresponding author for the article.

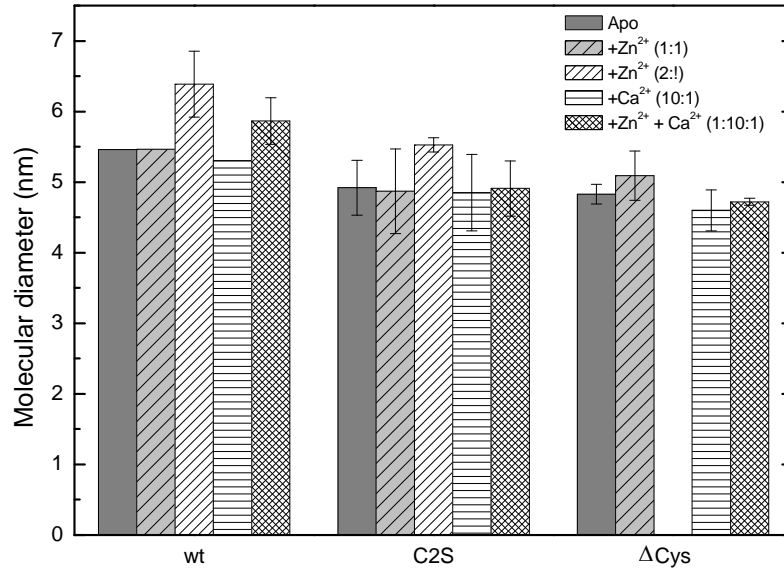


Figure S1: Molecular diameter of the apo and metallated S100A2 variants as assessed by DLS. When available, results are average \pm standard deviation of at least 3 replicate measurements. Sizes are derived from the volume-averaged distribution of sizes. There is no measurement of S100A2- Δ Cys +2 Eq Zn²⁺ because the protein aggregates.